NASA TECHNICAL MEMORANDUM

NASA TM X-1154

TELEMETRY MEASUREMENTS OF AFTERBODY PRESSURES ON FREE-FLYING MODELS OF THE APOLLO CAPSULE AT MACH NUMBERS FROM 10 TO 21 IN HELIUM AND 14 IN AIR

by Joseph H. Kemp, Jr.

Ames Research Center
Moffett Field, Calif.

NATIONAL AERONAUTICS AND SPACE ADMINISTRATION • WASHINGTON, D. C. • OCTOBER 1965

NASA TM X-1154

TELEMETRY MEASUREMENTS OF AFTERBODY PRESSURES ON FREE-FLYING MODELS OF THE APOLLO CAPSULE AT MACH NUMBERS FROM 10 TO 21 IN HELIUM AND 14 IN AIR

By Joseph H. Kemp, Jr.

Ames Research Center
Moffett Field, Calif.

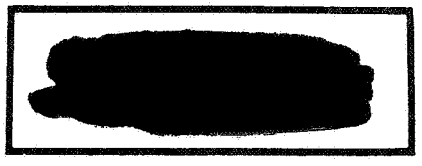

NATIONAL AERONAUTICS AND SPACE ADMINISTRATION

TELEMETRY MEASUREMENTS OF AFTERBODY PRESSURES ON FREE-FLYING MODELS OF THE APOLLO CAPSULE AT MACH NUMBERS FROM 10 TO 21 IN HELIUM AND 14 IN AIR*

By Joseph H. Kemp, Jr.
Ames Research Center

SUMMARY

20056

A telemetry system has been used to measure afterbody pressures on free-flying wind-tunnel models of the Apollo Command Module. These measurements were made in the Ames 14-inch and 20-inch hypersonic helium tunnels at Mach numbers of 10, 15, and 21 and in the Ames 1-foot shock tunnel at a Mach number in air of 14. The corresponding Reynolds numbers, based on model diameter, were 360,000, 1,150,000, and 975,000 in helium, and 11,800 in air.

Pressures were measured on the most windward side of the afterbody for angles of attack from 0° to -40° and comparisons were made between the data obtained from the free-flight tests and existing data obtained by various investigators using sting-mounted test models. In some cases the measurements obtained from sting tests agreed well with the present measurements obtained with free-flying models; but in other cases, the disagreement was as large as 30 percent. The differences observed in the measurements obtained with sting-mounted models probably were due primarily to differences in the types and geometry of the sting arrangements used. Substantial differences in the afterbody pressure measured in air compared with the afterbody pressure measured in helium were also observed. These differences were found to be strongly dependent on the angle of attack of the model and in agreement with theoretical trends. Conf Author

INTRODUCTION

The existence of unknown, and possibly large, model-support-interference effects has been a troublesome problem in experimental testing in wind tunnels. The interference effects are difficult to evaluate at hypersonic speeds, especially in studies of base flows or flows over afterbodies of entry shapes such as the Apollo capsule.

The recent development of a telemetry system, reported in reference 1, for measuring pressures on test models in free flight, has made it possible to obtain pressure measurements free of support interference. This pressure telemetry system was used to obtain pressures on the afterbody of Apollo type test models at hypersonic Mach numbers and the results of these tests are

---

[redacted] Unclassified.

[redacted]

presented in this report. The present free-flight pressure measurements are compared with existing data obtained with sting-mounted test models.

NOTATION

C_D	drag coefficient
c.g.	center of gravity
d	model diameter
M_∞	free-stream Mach number
p	pressure, psi
$\overline{p}_1$	driving pressure in model launcher
p_b	model afterbody pressure
p_{t_2}	total pressure behind normal shock
p_∞	free-stream static pressure
Re	free-stream Reynolds number, based on model diameter
r_c	corner radius of the model
r_n	front-face radius of the model
s	surface distance measured from stagnation point at zero angle of attack
T_t	free-stream total temperature
T_w	model wall temperature
t	time
$\overline{u}_1$	launch velocity of test model, ft/sec
α	angle of attack, deg
γ	specific heat ratio
θ_a	afterbody angle of the model

Test Facilities

Three facilities were used in the present investigation, the Ames 14-inch and 20-inch hypersonic helium tunnels and the Ames 1-foot shock tunnel. The 14-inch helium tunnel was used for tests at Mach numbers 10 and 21 while the 20-inch helium tunnel was used for tests at Mach number 15. These tunnels, described in detail in references 2 and 3, are blowdown tunnels with interchangeable axially symmetric nozzles. Tests at Mach number 14 in air were conducted in the 1-foot shock tunnel. This tunnel, described in reference 4, operates at a test-section stagnation enthalpy of about 4600 Btu/lb and a free-stream Mach number of approximately 14. The test times in this tunnel range up to 20 milliseconds.

Model Launching Apparatus

In the helium tunnels the models were launched by a pneumatic launcher similar to the one described in reference 5. This launcher was installed in the tunnel downstream of the test section. The launcher is shown schematically in figure 1 and photographs of the launcher installed in the 14-inch helium tunnel are shown in figure 2. The pneumatic launcher consisted of a piston and rod on which was placed a cup-like holder for support of the model during launch. The piston was contained in a tube and "firing" of the test model was accomplished by releasing a restraining pin. The upstream side of the piston was vented to tunnel static pressure while the downstream side was subjected to the driving pressure, $\bar{p}_1$, which was set at a predetermined value so that the upstream portion of the model trajectory terminated near the upstream edge of the viewing window. (A method for estimating the required pressure, $\bar{p}_1$, for the launcher is described in the appendix of this report.)

A necessary requirement for the pneumatic launcher in the present experimental program was the capability of launching test models without imparting rolling or yawing motion. High-speed motion pictures of a number of free-flying models were studied and it was clearly evident that the rolling or yawing motion induced by the launching process was less than 0.2°.

In the 1-foot shock tunnel, the test models were simply suspended by small nylon threads which burn away at the start of the flow, thereby releasing the model into a free-flight condition. A photograph of a typical test model suspended by threads in the shock tunnel is shown in figure 3.

Models

The basic geometry of the test models and the location of the afterbody pressure orifice are shown in figure 4. The outer shell of the models was made in two sections as shown by sketches and photographs in figures 5 and 6. The

front section was made of brass with provision for a solder filler so that the location of the center of gravity could be retained on the model axis or offset vertically.

The forward portion of the test models not only provided the proper ballasting but, in the case of the shock tunnel, it also served as a shield to eliminate the coupling between the plasma, in the shock layer of the model, and the telemetry unit (see discussion in ref. 1).

In the helium tunnels the models were launched at zero angle of attack, and by offsetting the center of gravity a pitching oscillation in the free-flight motion was obtained which allowed pressure measurements to be made through a wide angle-of-attack range. This technique could not be used in the shock tunnel because of the limited test time available. Thus in order to obtain pressure data throughout the desired angle-of-attack range in the shock tunnel, test models were initially suspended at various angles of attack.

The two sections of the models were threaded together and sealed so that the inner portion of the model formed a sealed cavity in which a known pressure could be maintained. This pressure then served as a reference pressure for the pressure cell. In the helium tunnel tests the reference pressure was established in the model by using a hypodermic needle which passed through the model holder (see fig. 1) and then was inserted through a small rubber disk at the rear of the model (see fig. 5(a)). The reference pressure line to the needle was restrained so that the needle was extracted as the model was launched. In the shock tunnel the reference pressure was made equal to the pressure in the test section, immediately prior to the initiation of the run, by means of a 0.010-inch-diameter "vent" tube installed in the back of the model (see fig. 5(b)). Tests showed that the vent tube restricted the flow of air sufficiently that no significant change in the reference pressure occurred within the short test time of the shock tunnel.

Pressure Telemetry System

The telemetry units and pressure cells were the same as those described in reference 1. The telemetry unit consists of a miniaturized oscillator which is frequency modulated by a variable capacitance pressure cell. The FM receiver had a tuning range of 105 to 140 mc and a usable deviation bandwidth for information content of ±0.8 mc.

The sensitivities of the capacitance cells used were chosen to be compatible with the expected range of pressures to be measured and the deviation bandwidth available. The cells used to measure pressures at $\alpha = 0$ had a range of ±0.05 psi differential for a frequency deviation of 0 to 0.8 mc and the cells used to measure pressures at angles of attack had a range of ±0.5 psi differential.

Recording Equipment

In both the helium facilities and the shock tunnel the receiving antenna was mounted directly on the test-section windows. The demodulated signal from the FM receiver was recorded on a recording oscillograph using a galvanometer which had a flat frequency response range of 0 to 1200 cps.

The position and angle of attack of the free-flying models were recorded with a high-speed movie camera which was operated at a speed of about 2000 frames per second.

The recording oscillograph, the high-speed camera, and the model launcher were started in the proper sequence by an automatic control unit. This control unit also provided a time reference "pulse" which was recorded simultaneously on the camera film and the oscillograph record. This time reference mark, along with periodic timing marks on the camera film and the oscillograph record, were then used to correlate the model position and attitude with the telemetered pressure data.

TEST AND PROCEDURES

Test conditions are shown in the following table:

M_∞	Test gas	Re	T_w/T_t
10	helium	360,000	1
15	helium	1,150,000	1
21	helium	975,000	1
14	air	11,800	.05

The estimated error of p_b/p_{t_2} due to instrument errors, gage accuracies, and repeatability of tunnel conditions is ± 0.001 at $\alpha = 0$ and ± 0.0025 at $\alpha \neq 0$, while the estimated error in angle is $\pm 0.2^\circ$ at $\alpha = 0$ and $\pm 1^\circ$ at $\alpha \neq 0$. The higher error in angle for $\alpha \neq 0$ is due to possible errors in time correlation of ± 0.0005 sec.

Typical Data Records

A typical oscillograph trace of the telemetered data and related frames from the motion pictures are shown in figure 7 for a test run in the 14-inch helium tunnel using a model with the c.g. on the model axis. A sketch of the tunnel test section showing the trajectory of the model is also included in figure 7. The relative high pressure measured at the beginning of the free-flight trajectory, point A of figure 7, is believed to be due to interference between the wake of the model and the model launcher. As the model moves upstream it appears from the change in pressure that the wake suddenly closes and the interference-free base pressure reading is obtained (from

points B to C of fig. 7). The point at which the wake closed was approximately 7 model diameters forward of the extended model launcher.

A typical data record and photographs for a test run using a model with the c.g. displaced vertically from the model axis are presented in figure 8. Also included in this figure is the angle-of-attack history, obtained from the motion-picture film, for the model when it is in the viewing area of the test section. For this particular run afterbody pressure data were obtained in the angle range of about -25° to -45°.

RESULTS AND DISCUSSION

The measured values of afterbody pressure, p_b, normalized using free-stream impact pressure, p_{t_2}, are presented as a function of angle of attack in figure 9 for free-flight tests in helium flow and in figure 10 for free-flight tests in air in the shock tunnel. In figure 9, the data obtained with pitching models have been faired and arrowheads inserted to indicate the order of data acquisition.

From this figure it is apparent that the differences obtained for the model increasing in angle of attack and data obtained during the same run with the model decreasing in angle of attack are small, while differences between runs are slightly larger but still within the estimated accuracy of the data.

Although in the helium tunnels the pitching models were launched at $\alpha = 0^{\circ}$, data were in general not obtained for angles of attack in the range near 0° to about -15° because of the interference of the model-launching apparatus with the model base flow field during the initial portion of the trajectory where the model angle of attack is small. Data were obtained, however, for angles of attack from -5° to -15° in one of the tests in the 20-inch helium tunnel (see fig. 9(b)). In this case the measured base pressures in the angle-of-attack range from about -5° to about -15° appear to be somewhat lower than the pressure at $\alpha = 0^{\circ}$. This behavior has been noted by other investigators (see, e.g., ref. 6) but at this time the reasons for this phenomenon are still unknown.

Variation in Afterbody Pressure With Mach Number

The variations in afterbody pressure with Mach number for the tests in helium, obtained from cross plots of figure 9, are presented in figure 11 for a number of angles of attack. From this figure it is apparent that within the scatter of the data for a given α there is no significant variation in the ratio of base pressure to free-stream impact pressure for the Apollo capsule over the Mach number range from 10.1 to 21.

Comparison of Results Obtained in Air and Helium

A comparison of afterbody pressure measurements obtained in helium and air is made in figure 12. The measurements made in these two gases were at considerably different Reynolds numbers and stream enthalpy levels but the comparisons made are considered valid in light of the data presented in figure 9 of reference 7. Those data showed that the afterbody pressure on the Apollo capsule is relatively unaffected by variations in Reynolds numbers from 6×10^3 to 2.3×10^6 or by variations in stream enthalpies from 130 Btu/lb to 4000 Btu/lb. Also shown in figure 12 are theoretical values of the afterbody pressure for $\alpha = 0^\circ$ obtained using the method of Denison and Baum (ref. 8) and for $\alpha = -33^\circ$ obtained using two-dimensional blast-wave theory as used in reference 7 and C_D values of 0.97 for helium and 1.03 for air.

At $\alpha = 0$ Denison and Baum theory predicts values which agree very well with experimental data for both air and helium, while at $\alpha = -33^\circ$ blast-wave theory agrees reasonably well with the experimental data.

From both experiment and theory it is apparent that at $\alpha = 0$, the Apollo afterbody pressure obtained for tests in air is nearly twice the value obtained for tests in helium. This difference between the air and helium data decreases as the model pitches until at about $\alpha = -30^\circ$ the data curves cross and the value for tests in helium becomes higher than the value for tests in air. This crossing of the data curves is predicted by blast-wave theory which indicates that at $\alpha = -33^\circ$ the pressure in air should be lower than the pressures in helium.

Comparisons of Data for Free-Flying and Sting-Mounted Models

Presented in figures 13 and 14 are comparisons between the present data obtained with free-flying models and data from sting-mounted models presented in references 6, 7, 9, 10, and 11. All values given are for pressure measurements at the midpoint of the model afterbody, ($s/d = 0.95$) except for reference 10 where the pressure orifice was located about 10 percent of the afterbody length farther back. The front-face radius, the corner radius, and the afterbody angle of the test models along with Mach number, Reynolds number, and wall temperature ratio for all data in figures 13 and 14 are given in table I.

The base pressures obtained by telemetry from free-flying models at α near 0 (figs. 13 and 14) are generally equal to or less than those obtained using sting-mounted models whereas at angles of attack less than about -15° (fig. 14) the free-flight data are generally equal to or greater than the data obtained with sting-mounted models. Although in some cases there is good agreement between free-flight and sting-mounted data, for other cases the disagreement was as large as 30 percent. It is noted that although there is considerable variation in Mach number, Reynolds number, and wall temperature ratio of the data being compared (table I), there appears to be no obvious correlation between these parameters and the differences in the data. Therefore it is felt that the differences in data obtained for a given test

gas are primarily due to differences in the types and geometry at the sting arrangements used. In general, it appears that, if proper care is taken, readings of afterbody pressure reasonably free of sting interference can be obtained with sting-mounted models, at least for blunt shapes. However, the free-flight, telemetry technique offers a more reliable method for obtaining values on the afterbody of blunt configurations.

CONCLUDING REMARKS

Measurements of the afterbody pressure on free-flying test models of an Apollo capsule in air and helium have been made using an FM telemetry system. It was found that the ratio of afterbody pressure to free-stream impact pressure for a given angle of attack did not vary appreciably with Mach number over the Mach number range from 10 to 21. Comparisons were made between the measured values and theoretical values obtained by the method of Denison and Baum at $\alpha = 0^{\circ}$ and between measured values and theoretical values obtained by blast-wave theory at $\alpha = -33^{\circ}$. Good agreement was obtained between experiment and theory for both theoretical cases presented.

Substantial differences in the level of the afterbody pressure in air and helium were observed, the magnitude of the differences being strongly dependent on the model angle of attack. At angles of attack near zero the afterbody pressures in helium are substantially lower than in air as is predicted by Denison and Baum theory. At large negative angles of attack, the reverse is true; the afterbody pressure on the most windward side is higher in helium than in air, as indicated by blast-wave theory.

The present experimental results, obtained from free-flying models by telemetry, were compared with published results obtained by several investigators using sting-mounted test models. Differences as large as 30 percent were noted in the measurements probably because of differences in the types and geometry of the sting arrangements used. In some cases the measurements obtained from sting tests agreed closely with the present results obtained from models in free flight, indicating that reliable afterbody pressure measurements for blunt shapes can be made with sting-supported test models if sufficient care is taken. The difficulty, of course, is knowing when the interference effects have been minimized. The free-flight telemetry technique used in the present study provides a simple and direct means for obtaining afterbody pressures free of interference effects.

Ames Research Center
National Aeronautics and Space Administration
Moffett Field, Calif., July 13, 1965

[redacted]

APPENDIX

METHOD FOR ESTIMATING REQUIRED DRIVING PRESSURE

Estimates of the driving pressure, $\bar{p}_1$, for the pneumatic launcher used in the helium tunnels can be calculated as follows.

The velocity of the test model at launch, $\bar{u}_1$, and the time in seconds, t, needed to travel any required distance, $\bar{s}_1$, (see fig. 15) are governed by the relationships

$$\bar{u}_1 = \sqrt{\frac{2D\bar{s}_1}{m_m}} \tag{1}$$

$$t = \sqrt{\frac{2m_m\bar{s}_1}{D}} \tag{2}$$

where D is the aerodynamic drag of the model and m_m is the mass of the model. The time, t, is considered first and the maximum value is the time for a free-falling object to travel from rest at the vertical height, h_1, (see fig. 15) to the edge of the tunnel boundary layer. This defines the optimum ratio between the model mass m_m and the aerodynamic drag D which allows for maximum test time. The required launch velocity to achieve a forward trajectory of length $\bar{s}_1$ (see fig. 15) can be calculated from equation (1) and a procedure for estimating the driving pressure of the launcher is as follows.

The launch velocity is relatively small ($\bar{u}_1 < 100$ fps) and the reservoir pressure required to achieve this velocity may be estimated if the driving gas is assumed to remain in equilibrium and the expansion is isentropic during the launching process. Since $\bar{p}_2 \ll \bar{p}_1$ the effects of $\bar{p}_2$ were neglected. The launch velocity is related to the driving pressure by the relationship

$$\bar{u}_1^2 = \frac{2l_2}{m_m + m_p}\left[\bar{A}_p\bar{p}_1 f\left(\gamma\,\frac{\bar{l}_2}{\bar{l}_1}\right) - (D + D_f)\right] \tag{3}$$

and by using equation (1) we obtain a convenient expression for estimating the reservoir pressure

$$\bar{p}_1 = \frac{D[1 + (\bar{s}_1/\bar{l}_2)(1 + M_p/m_m)] + D_f}{\bar{A}_p f(\gamma,\ \bar{l}_2/\bar{l}_1)}$$

[redacted]

where (see fig. 15)

$\bar{A}_p$ cross-sectional area of the piston, ft^2

D_f friction drag within the launcher, lb

$\bar{l}_1$ length of reservoir, ft

$\bar{l}_2$ length of piston stroke, ft

M_p mass of piston ensembly including model holder, slugs

$\bar{p}_1$ reservoir pressure, lb/ft^2

$\bar{p}_2$ pressure on back face of the piston, lb/ft^2

and the energy function is given by

$$f\left(\gamma, \frac{\bar{l}_2}{\bar{l}_1}\right) = \frac{1}{(\bar{l}_2/\bar{l}_1)(\gamma - 1)} \left[1 - \frac{1}{1 + (\bar{l}_2/\bar{l}_1)^{(\gamma-1)}}\right]$$

where γ is the specific heat ratio. The energy available for various ratios of reservoir length to piston stroke is indicated in figure 16. It is evident that little is to be gained by using reservoir length larger than about twice the piston stroke. In the present application a piston diameter of 1 inch, a piston stroke of 6 inches, and a reservoir length of 12 inches were used in the 14-inch helium tunnel and piston diameter of 2 inches, a piston stroke of 9 inches, and a reservoir length of 18 inches were used in the 20-inch helium tunnel.

REFERENCES

1. McDevitt, John B.; Harrison, Dean R.; and Lockman William K : Measurements of Pressures and Heat Transfer by FM Telemetry From Free-Flying Models in Hypersonic Tunnel Streams. Paper presented at the First International Congress on Instrumentation in Aerospace Simulation Facilities, Paris, France, Sept. 28-29, 1964.

2. McDevitt, John B.; and Mellenthin, Jack A.: Characteristics of a Blunt Half-Cone Entry Configuration at Mach Numbers From 10.9 to 21.2 in Helium. NASA TM X-655, 1962.

3. Tendeland, Thorval; and Pearson, B. Douglas, Jr.: Effectiveness of Two Flap Controls on a Mercury Type Capsule at a Mach Number of 15 in the Ames Hypersonic Helium Tunnel. NASA TM X-660, 1962.

4. Cunningham, B. E.; and Kraus, S.: A 1-Foot Hypervelocity Shock Tunnel in Which High-Enthalpy, Real-Gas Flows Can Be Generated With Flow Times of About 180 Milliseconds. NASA TN D-1428, 1962.

5. Holway, H. P.; Herrera, J. G.; and Dayman, B., Jr.: A Pneumatic Model Launcher for Free-Flight Testing in a Conventional Wind Tunnel. JPL-TM-33-177, 1964.

6. Marvin, Joseph G.; and Kussoy, Marvin: Experimental Investigation of the Flow Field and Heat Transfer Over the Apollo-Capsule Afterbody at a Mach Number of 20. NASA TM X-1032, 1965.

7. Lee, George; and Sundell, Robert E.: Heat-Transfer and Pressure Distributions on Apollo Models at M = 13.8 in an Arc-Heated Wind Tunnel. NASA TM X-1069, 1965.

8. Denison, Richard M.; and Baum, Eric: Compressible Free Shear Layer With Finite Initial Thickness. AIAA J., vol., no.2, Feb. 1963, pp. 342-349.

9. Jones, Robert A.: Experimental Investigation of the Overall Pressure Distribution Flow Field, and Afterbody Heat-Transfer Distribution of an Apollo Reentry Configuration at a Mach Number of 8. NASA TM X-813, 1963.

10. Knox, E. C.: Heat-Transfer and Pressure Distributions Measured on the Apollo Command-Module Re-entry Configuration at Mach Number 19. AEDC-TDR-63-42, 1963.

11. Watson, Ralph.; and Wagner, Richard, D., Jr.: Pressure Distribution at a Mach Number of 24.5 on a Symmetrical Blunt-Faced Reentry Body at Angles of Attack From 0° to 40° in Helium Including an Investigation of Afterbody Sting Effects. NASA TM X-841, 1963.

TABLE I.- MODEL GEOMETRIC PARAMETERS AND TEST CONDITIONS FOR EXPERIMENTAL DATA PRESENTED IN FIGURES 13 and 14

Gas	Source	M_∞	Re	T_w/T_T	r_n/d	r_c/d	θ_a, deg
Helium	Ames 14-inch helium tunnel (present tests)	10 21	0.36×10^6 $.98\times10^6$	1 1	1.20 1.20	0.050 .050	33 33
	20-inch helium tunnel (present tests)	15	1.2×10^6	1	1.20	.050	33
	Ref. 6	20	1.9×10^6	1	1.20	.050	33
	Ref. 11	24.5	1.18×10^6	1	1.20	.050	35
Air	Ames 1-ft shock tunnel (present tests)	14	1.18×10^4	.05	1.20	.050	33
	Ames 1-ft shock tunnel (unpublished data)	10	1.25×10^4	.05	1.25	.052	33
	Ref. 8	13.8	3.5×10^4	.07	1.20	.050	33
	Ref. 9	8	1.36×10^6	>.5	1.20	.050	35
	Ref. 10	19	7×10^4	.09	1.20	.050	33

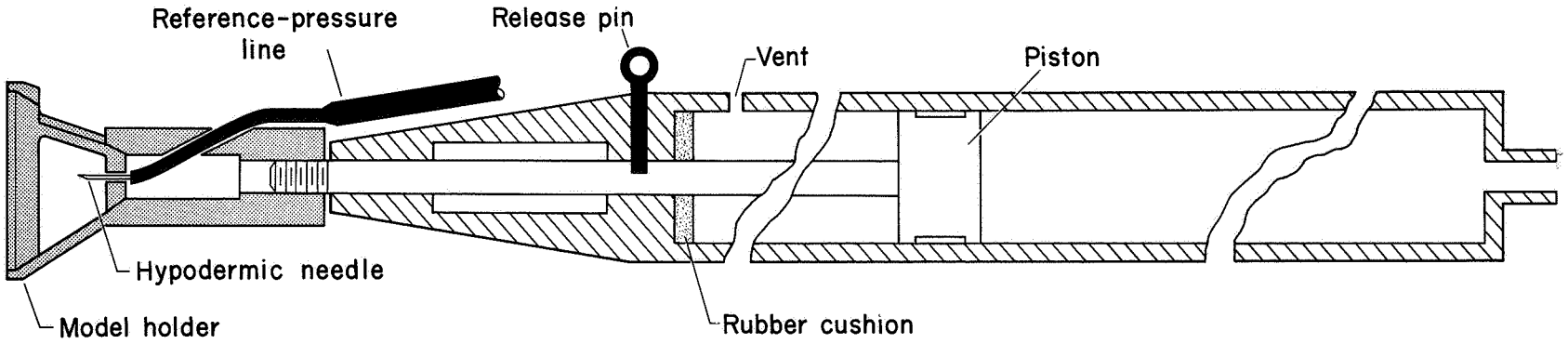

Figure 1.- Schematic of pneumatic launcher.

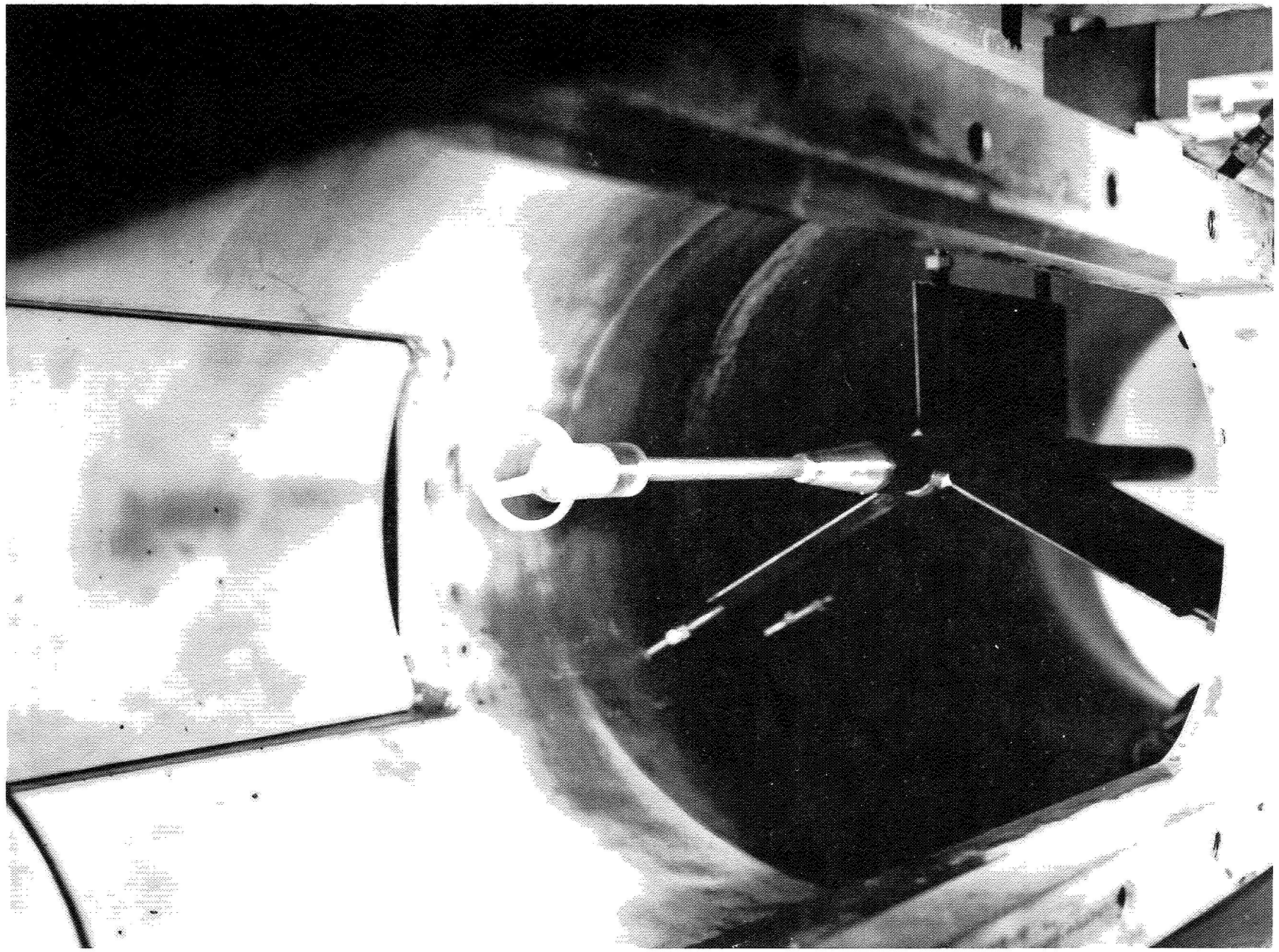

A-32073

Figure 2.- Photograph of the pneumatic launcher installed in the 14-inch helium tunnel.

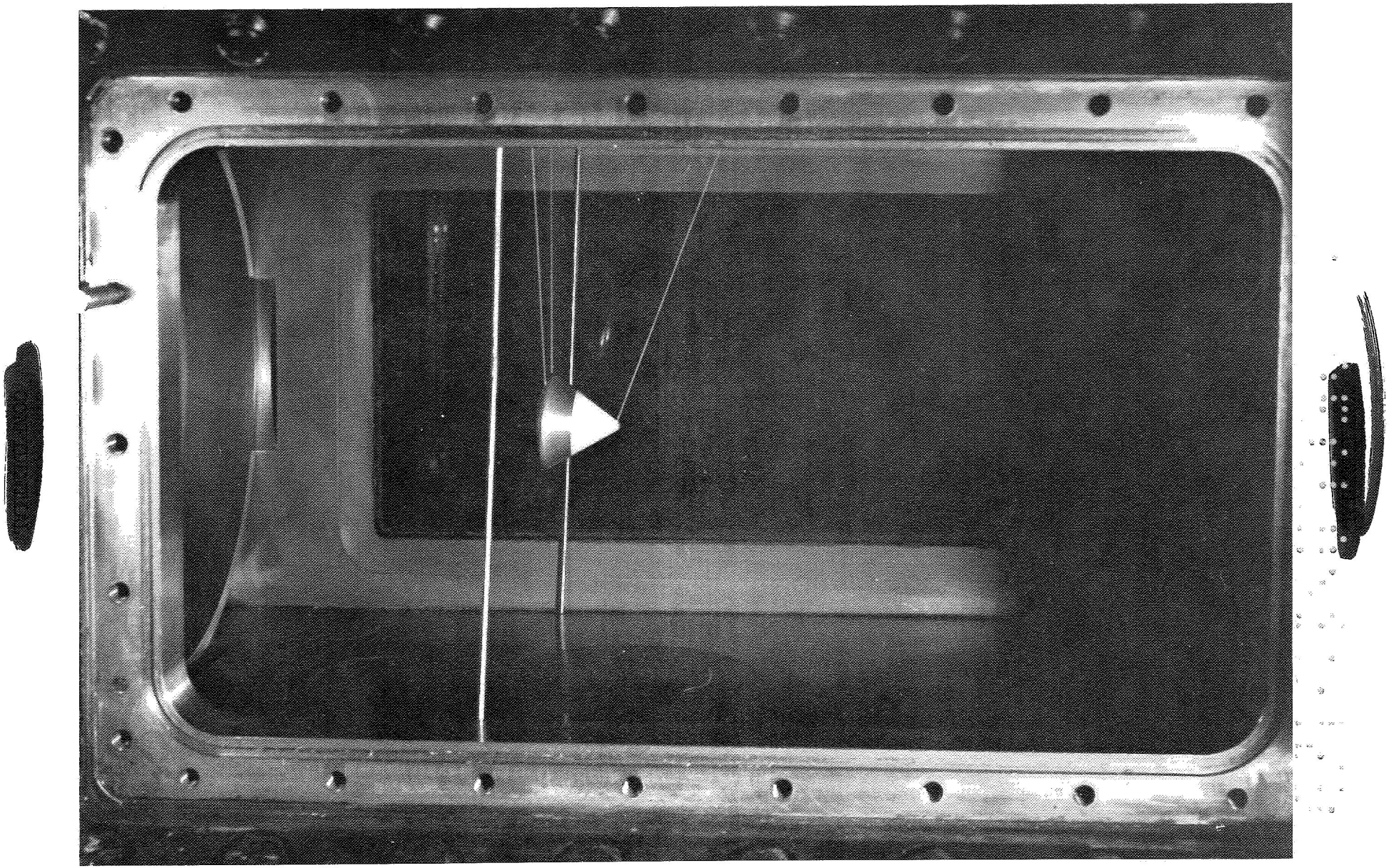

A-33794

Figure 3.- Photograph of test model suspended by threads in the 1-foot shock tunnel.

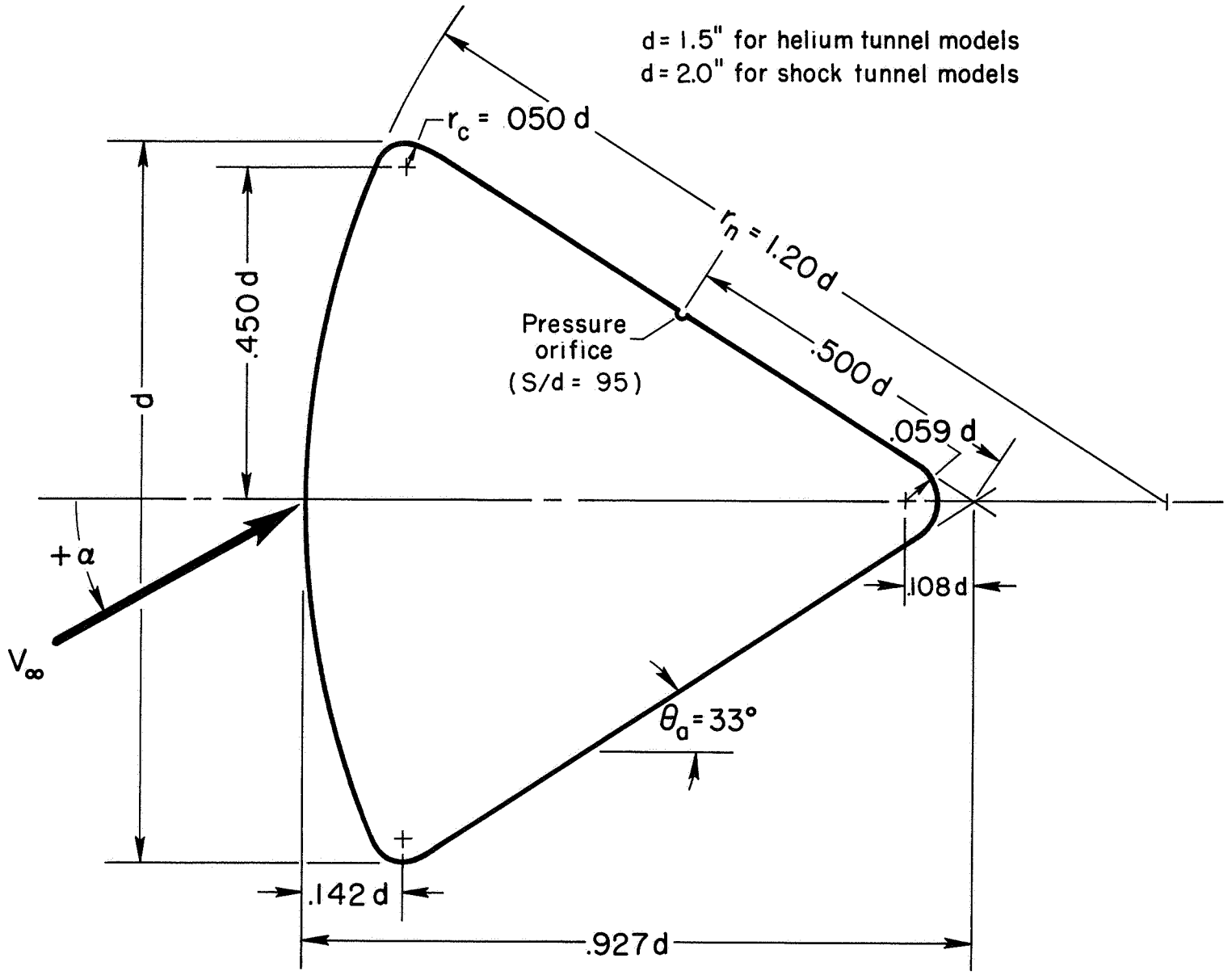

Figure 4.- Geometry of test models.

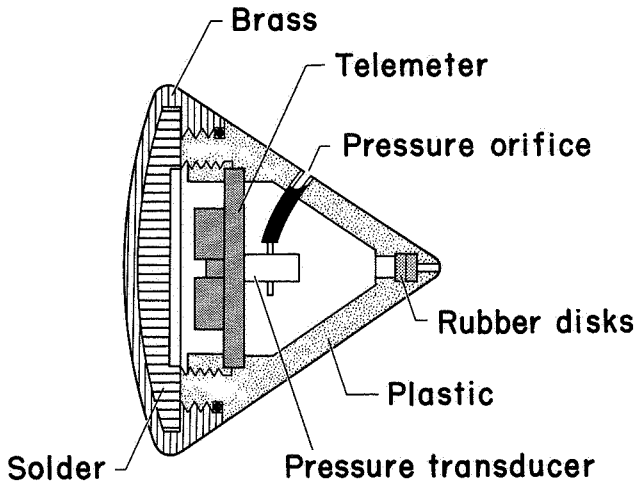

(a) Helium tunnel test models.

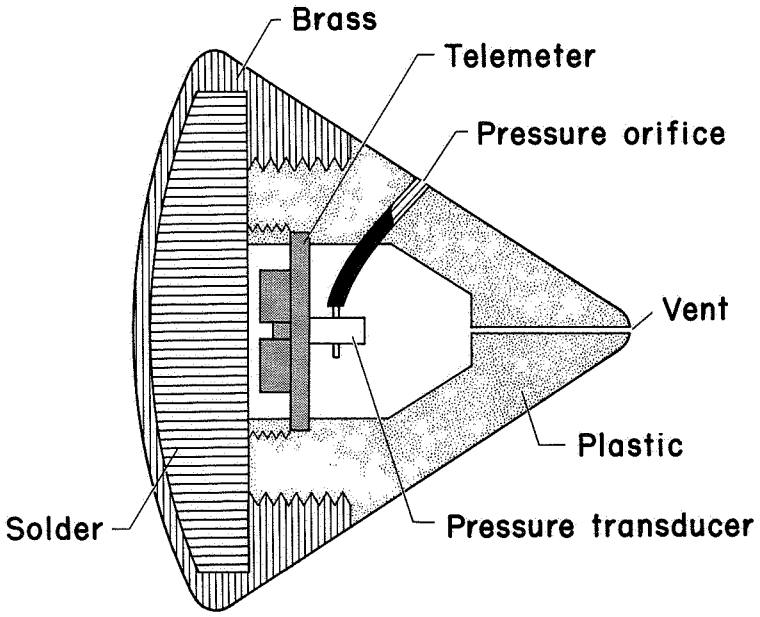

(b) Shock tunnel test models.

Figure 5.- Sketch of Apollo test models.

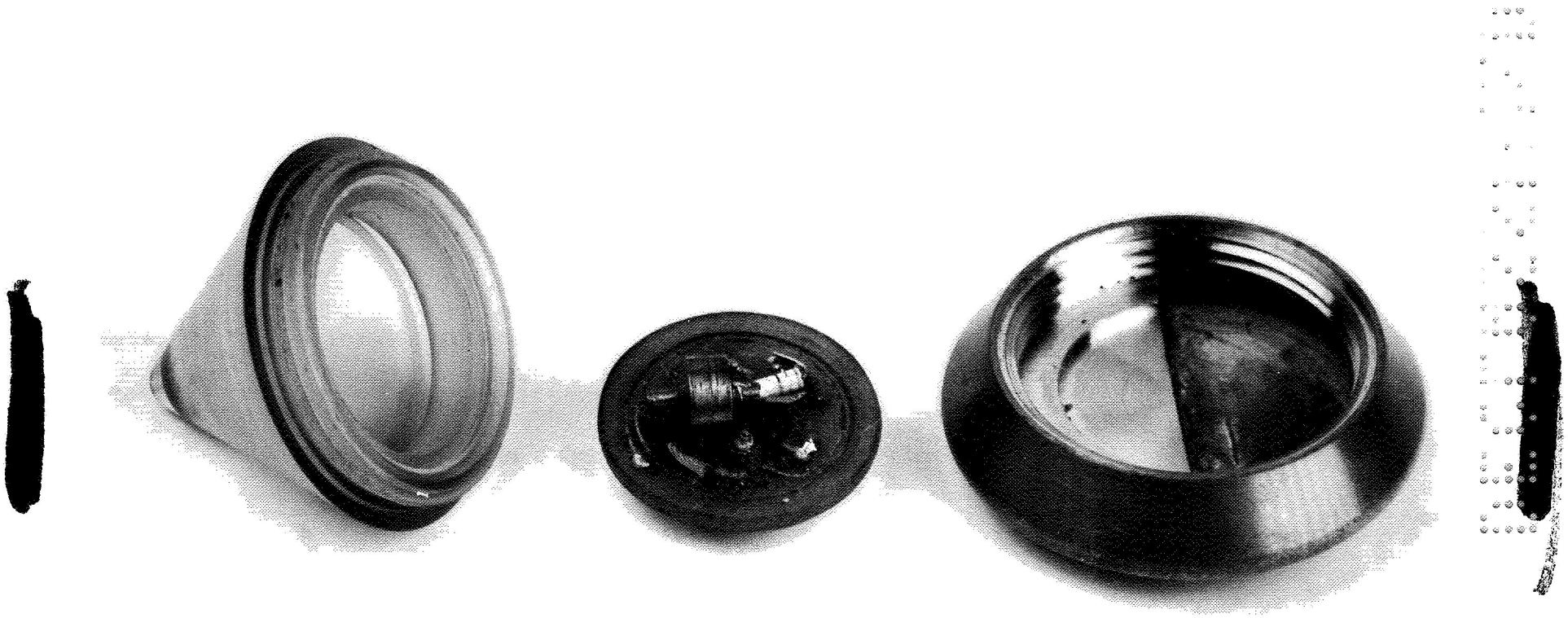

A-33792

(a) Helium tunnel test model with "offset" c.g.

Figure 6.- Photographs of test models.

A-33793

(b) Shock tunnel test model with centrally located c.g.

Figure 6.- Concluded.

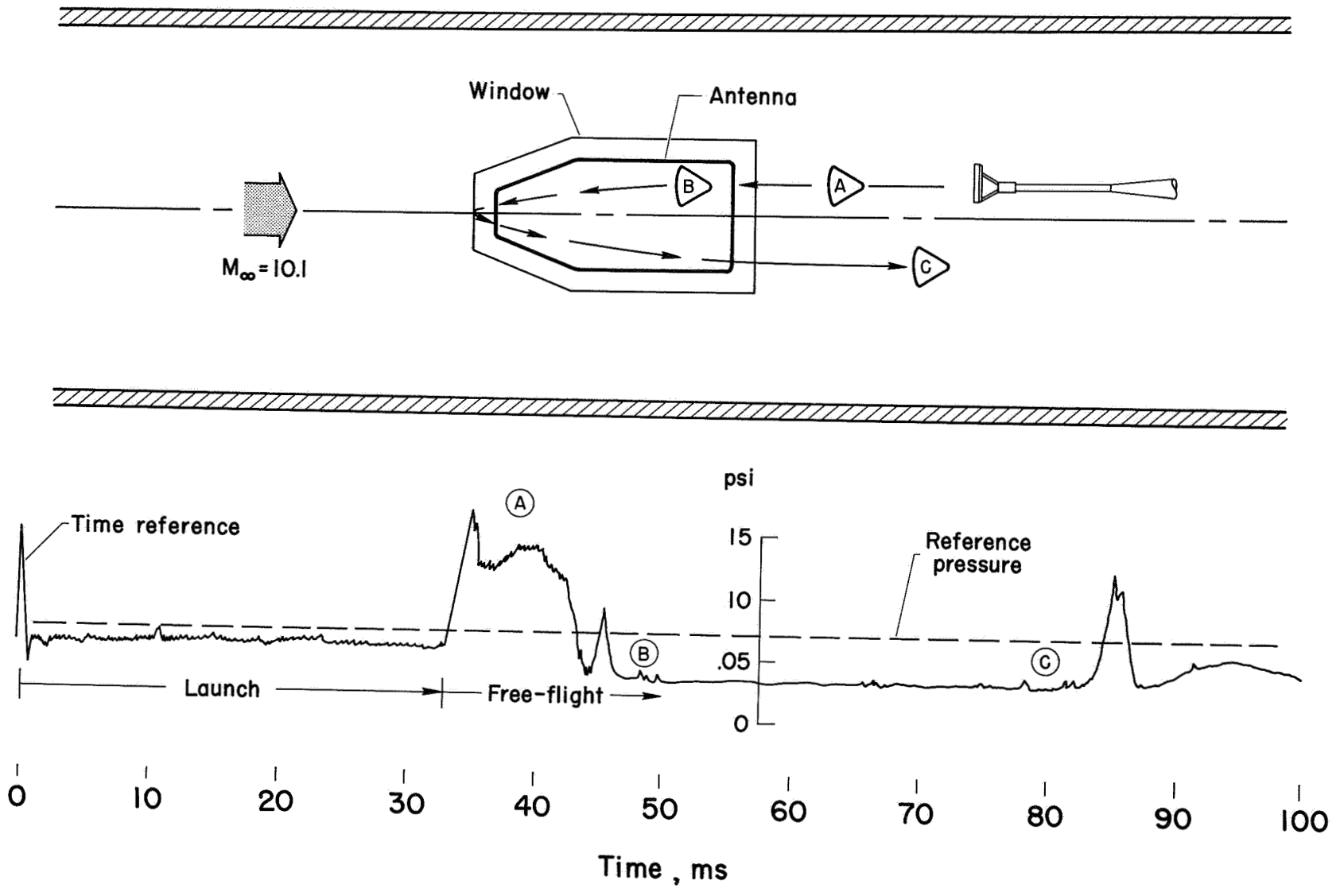

(a) Recording oscillograph trace of telemetry pressure signal.

Figure 7.- Typical data records for a free-flight model with the c.g. on the model axis; 14-inch helium tunnel, $M_\infty = 10.7$.

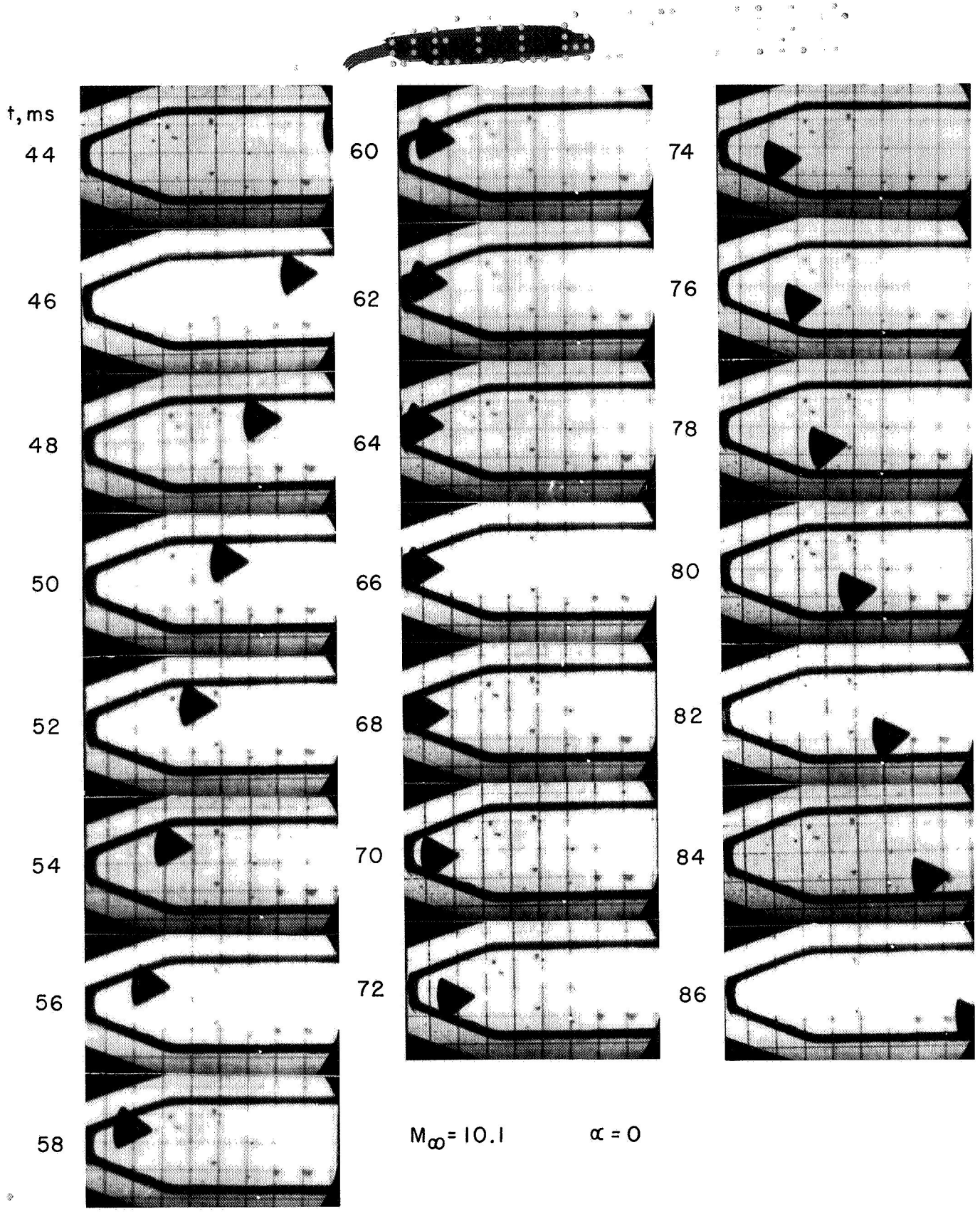

(b) Photographs of test model in free flight.

Figure 7.- Concluded.

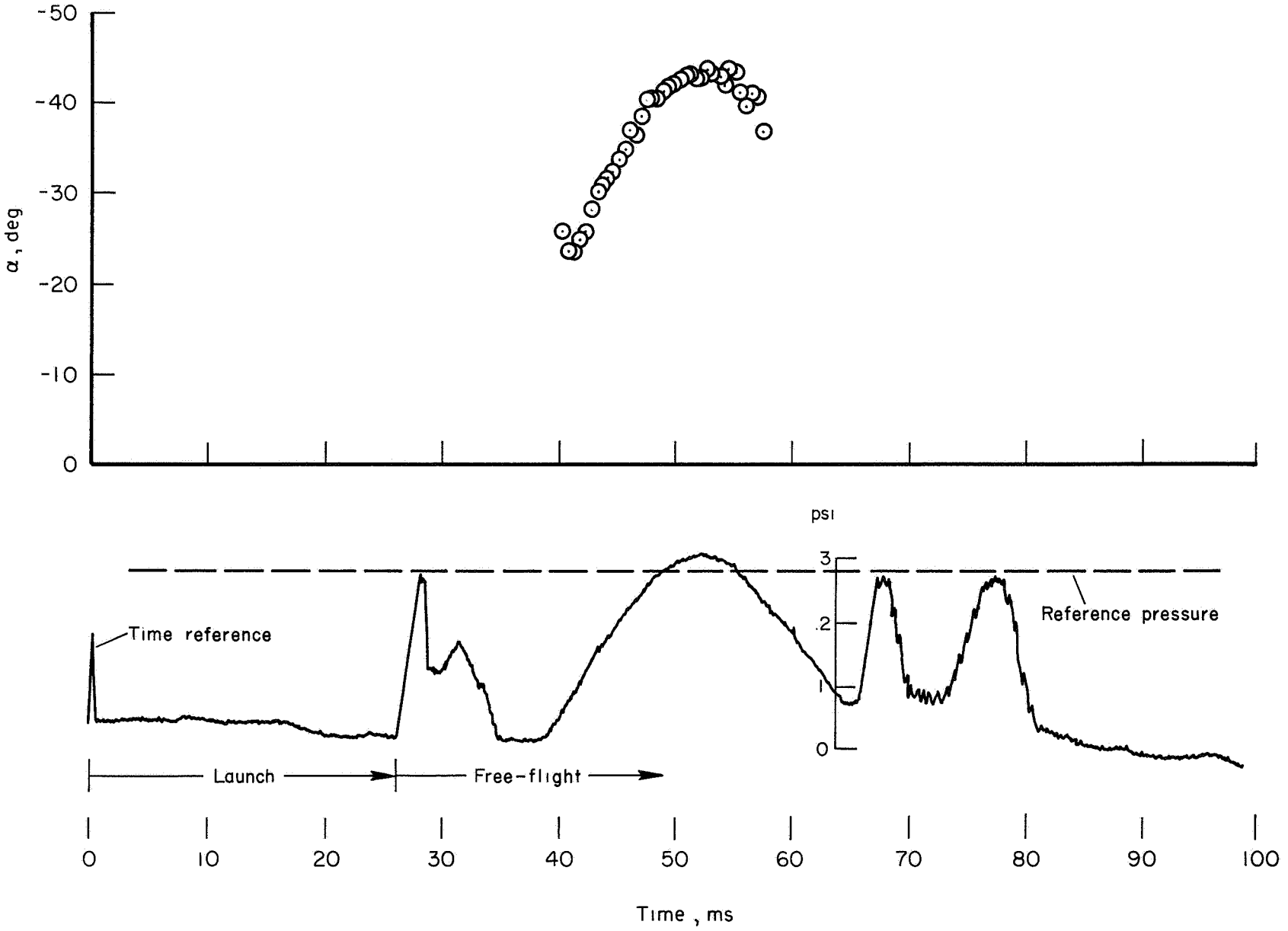

(a) Telemetry pressure signal and model angle-of-attack history.

Figure 8.- Typical data records for a free-flight model with c.g. offset from the model axis.

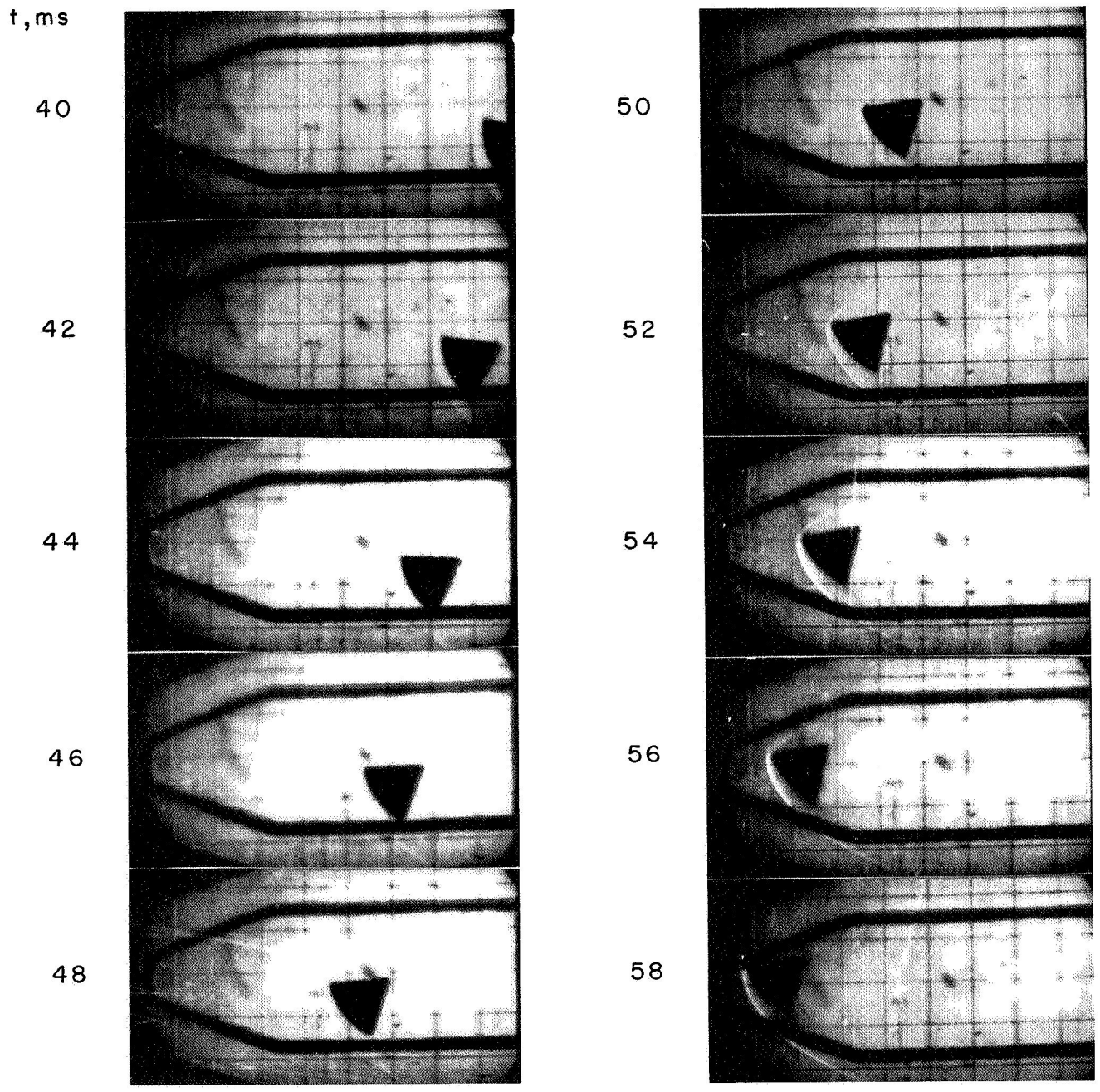

(b) Photographs of test model in free flight.

Figure 8.- Concluded.

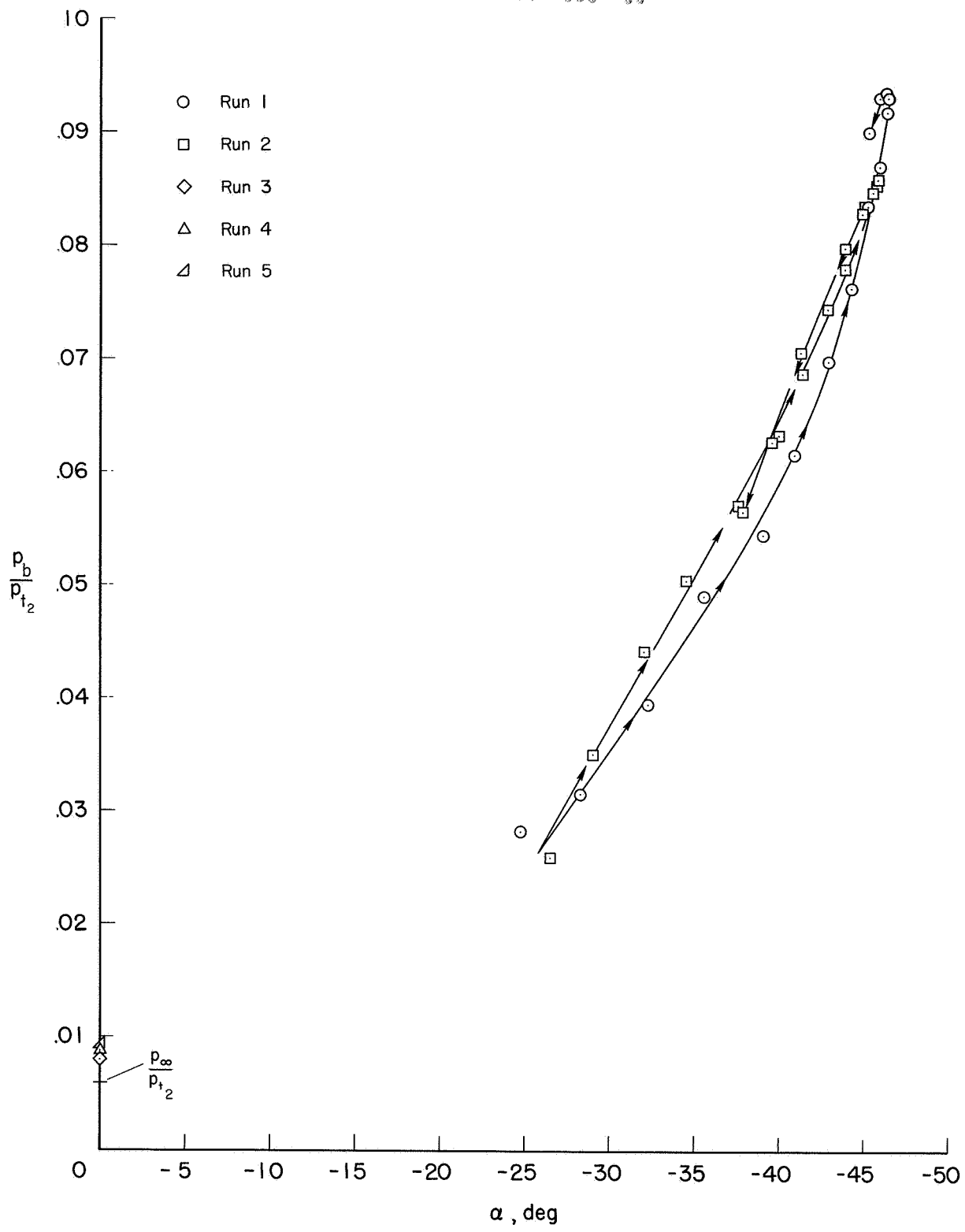

(a) $M_\infty = 10.1$.

Figure 9.- Free-Flight measurements of afterbody pressures in hypersonic helium flow.

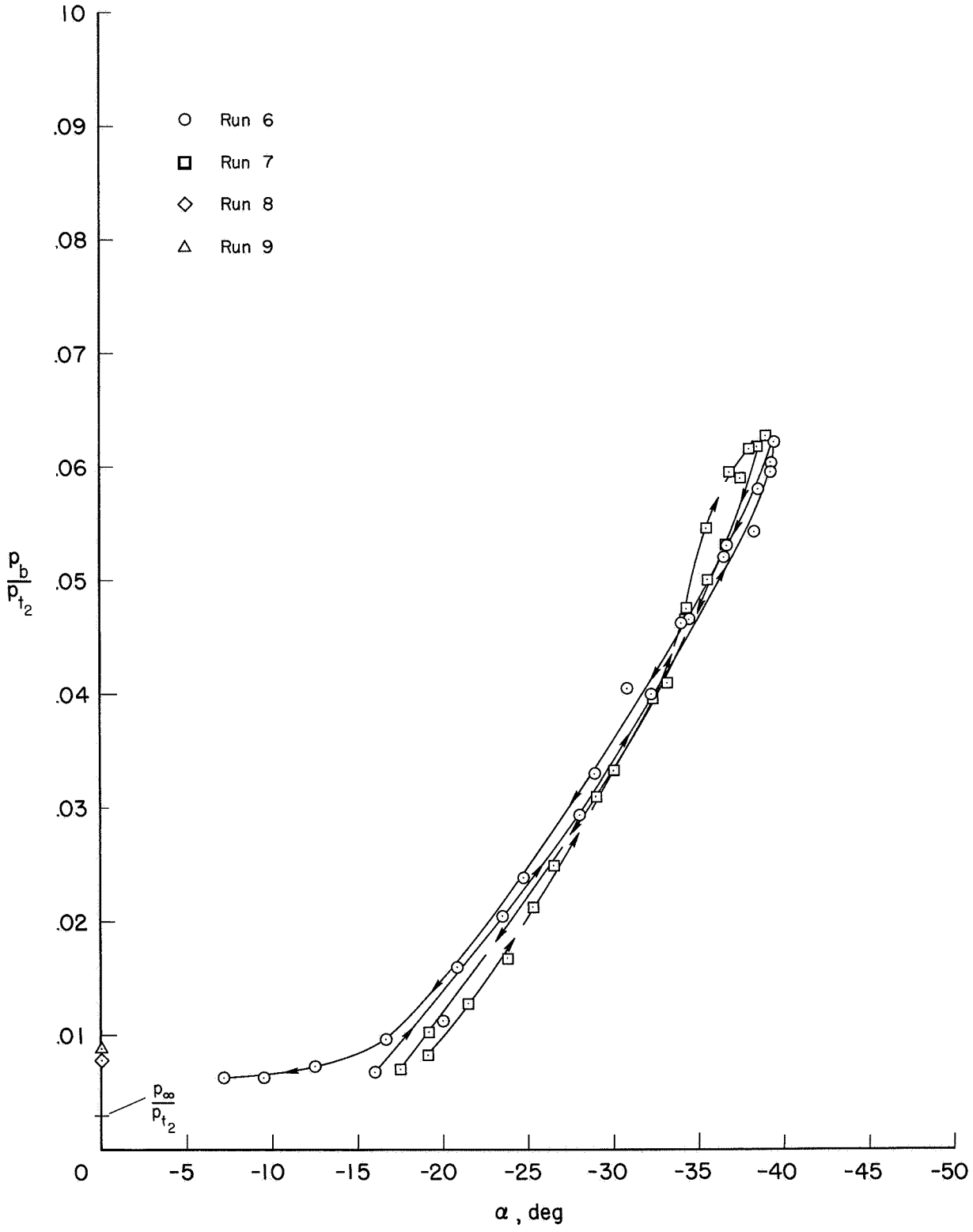

(b) $M_\infty = 15.0$.

Figure 9.- Continued.

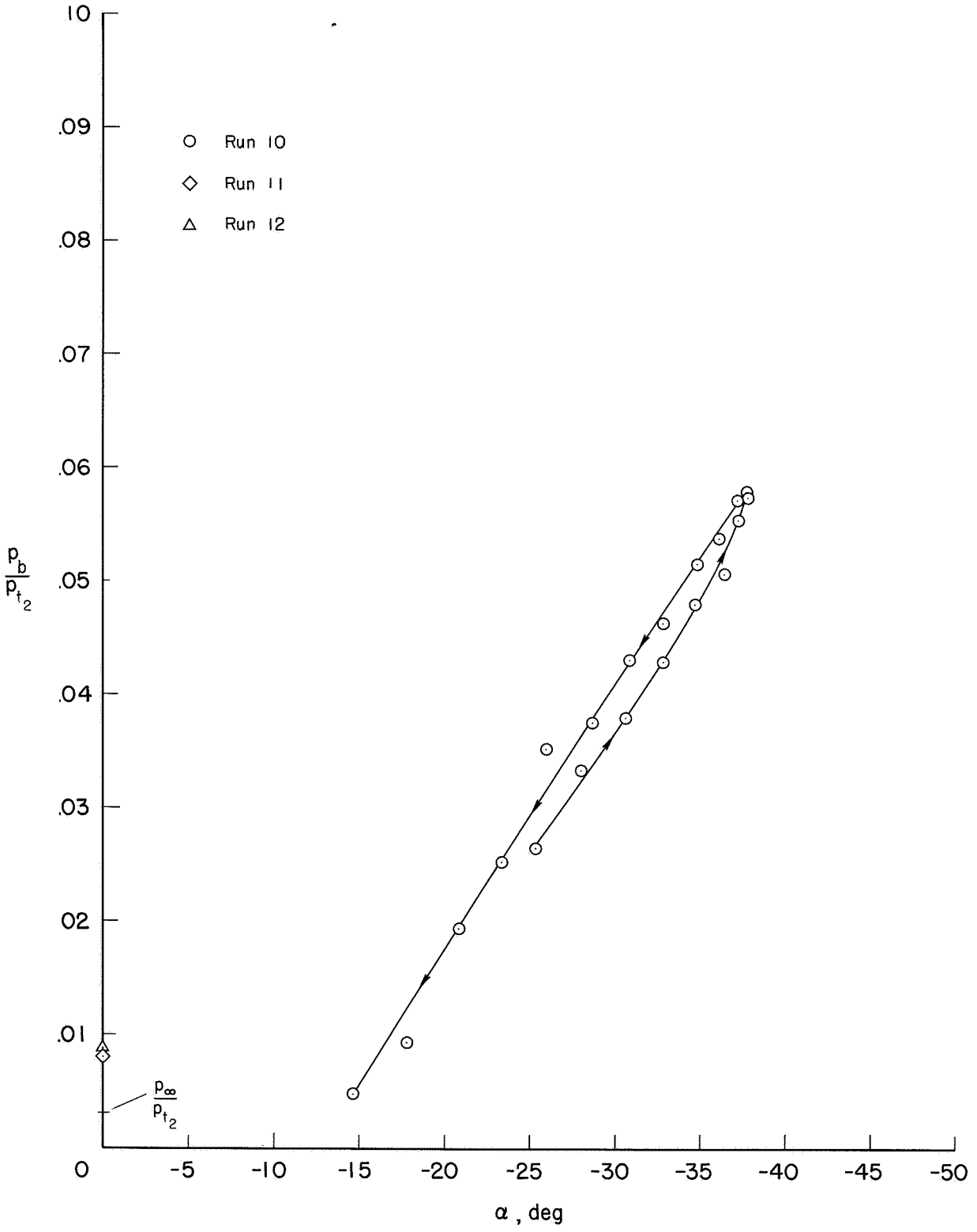

(c) $M_\infty = 21.0$.

Figure 9.- Concluded.

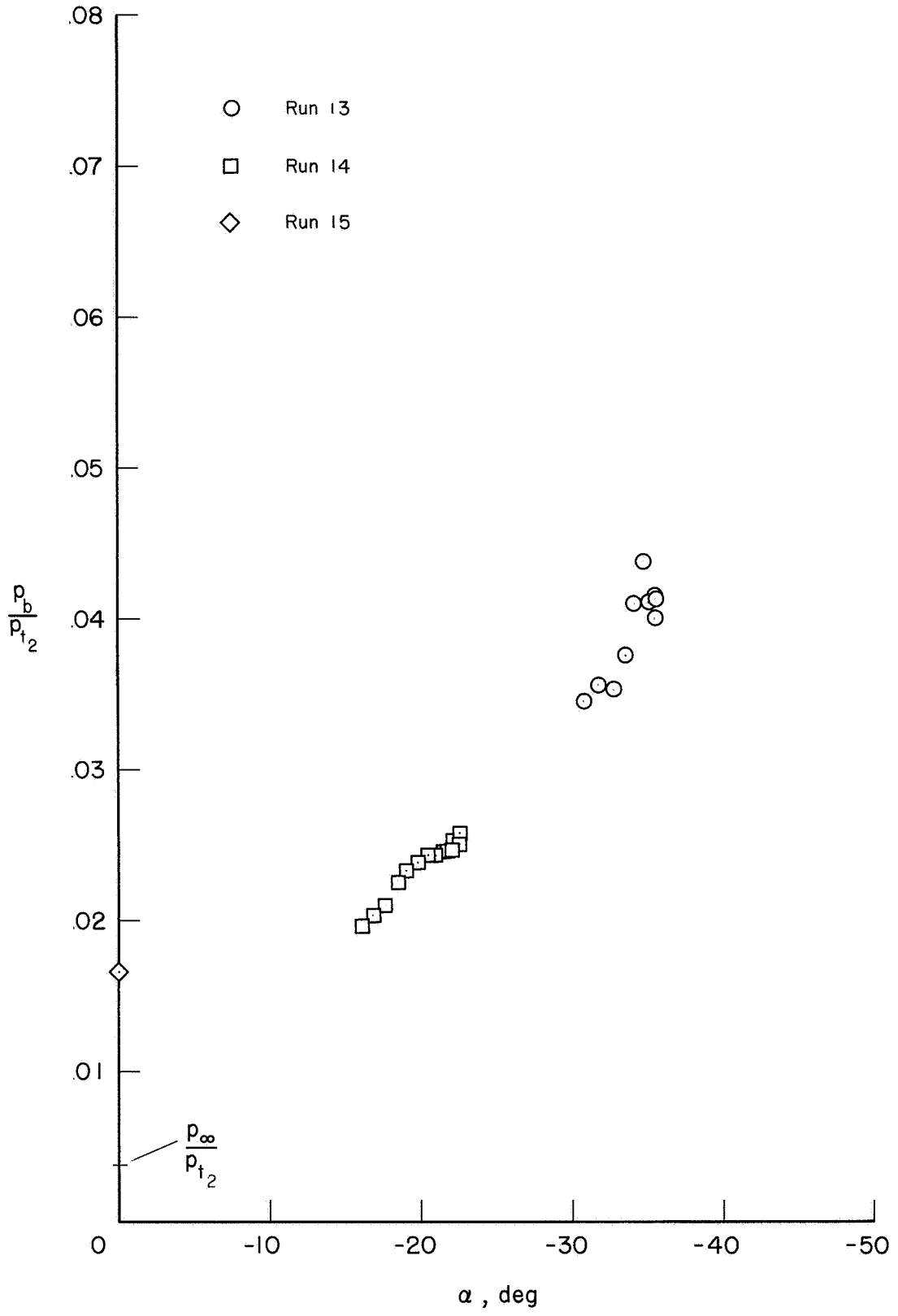

Figure 10.- Free-flight measurements of afterbody pressures in air at a Mach number of 14.

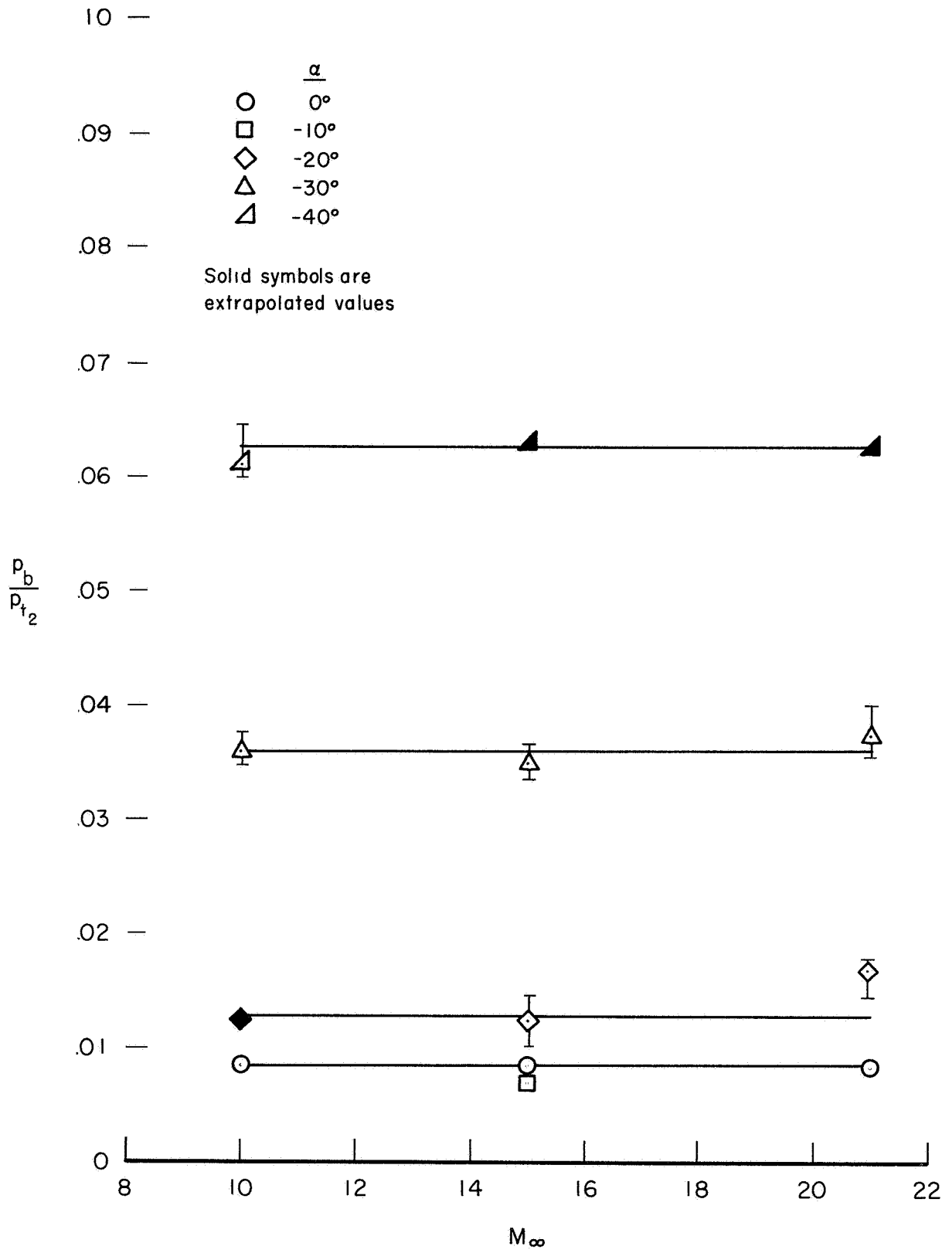

Figure 11.- Variations of afterbody pressures with Mach number in helium flow for various model angles of attack.

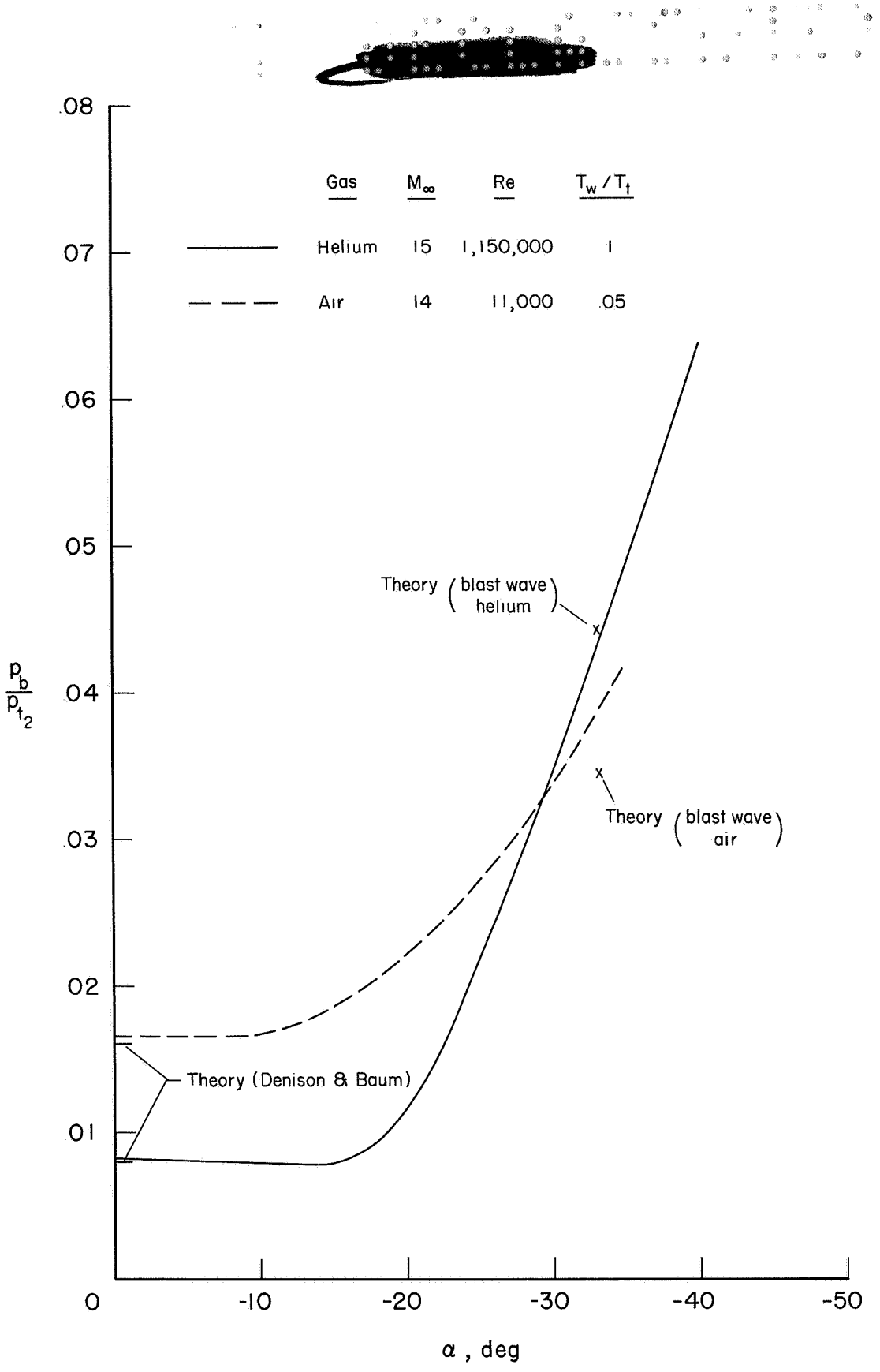

Figure 12.- Comparison of afterbody pressures in air and helium flow.

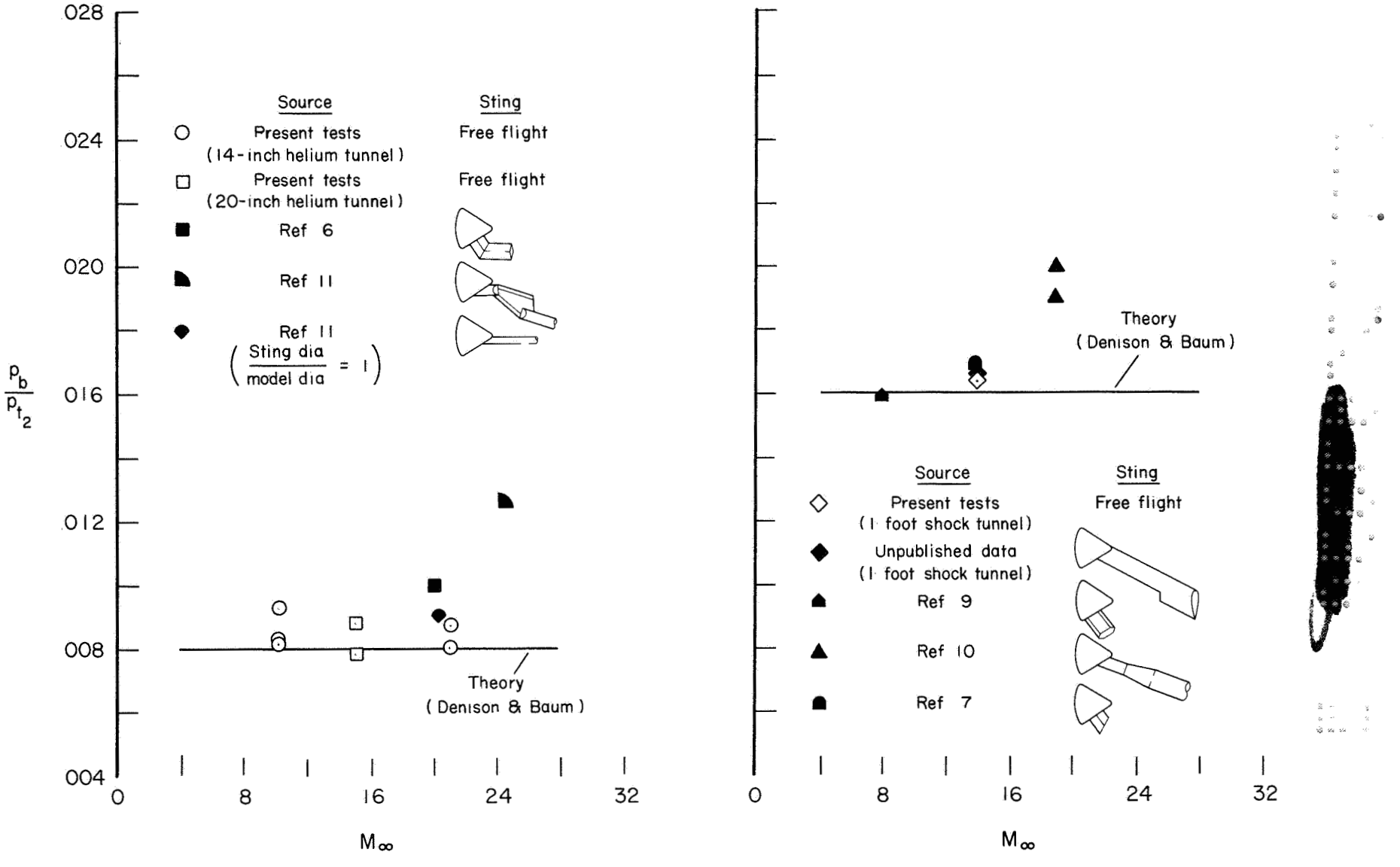

Figure 13.- Comparisons of afterbody pressure measurements with free-flying and sting-mounted models at $\alpha = 0$.

Helium

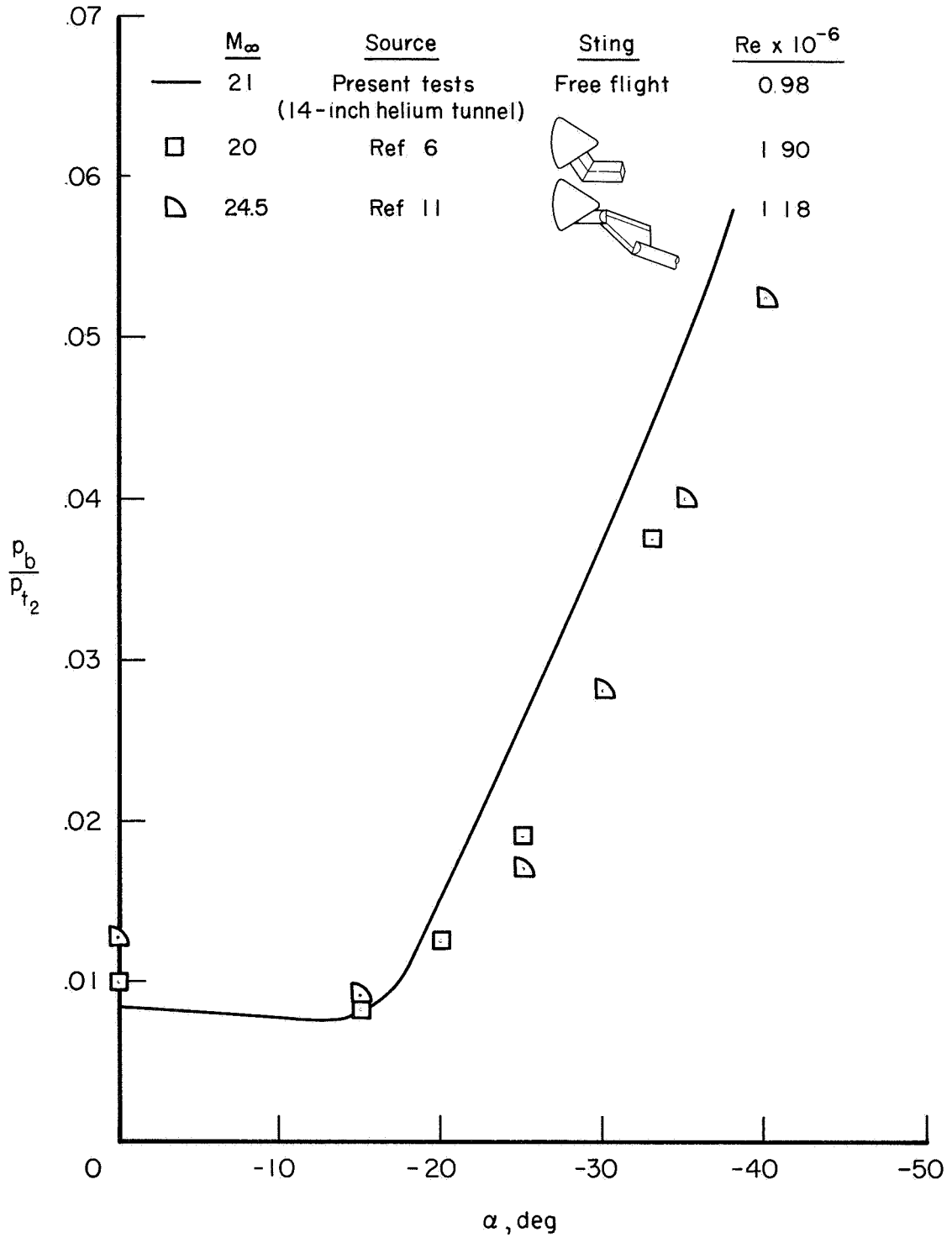

(a) Pressures in helium flow.

Figure 14.- Comparisons of afterbody pressure measurements with free-flying and sting-mounted models at various model angles of attack.

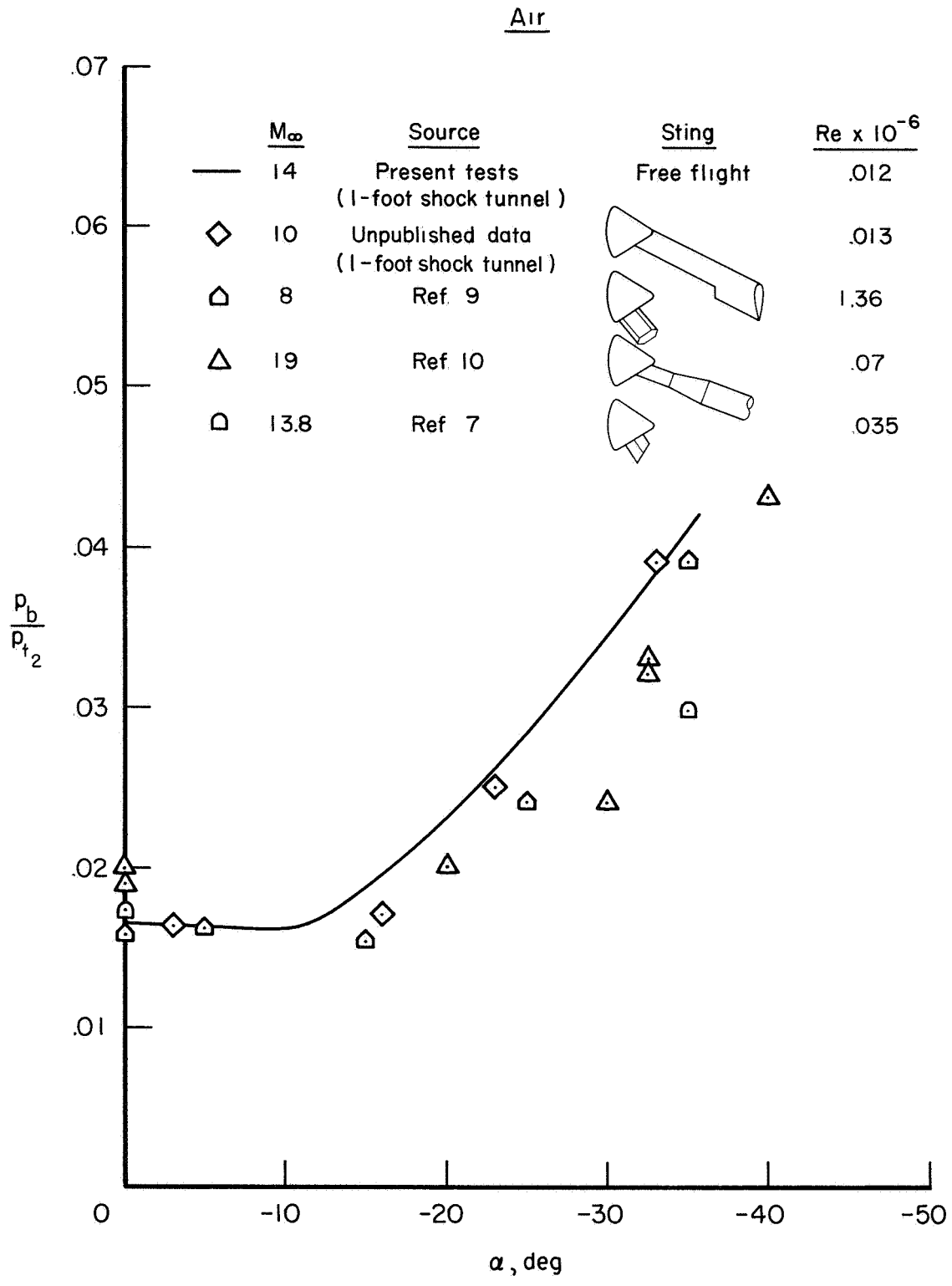

(b) Pressures in air flow.

Figure 14.- Concluded.

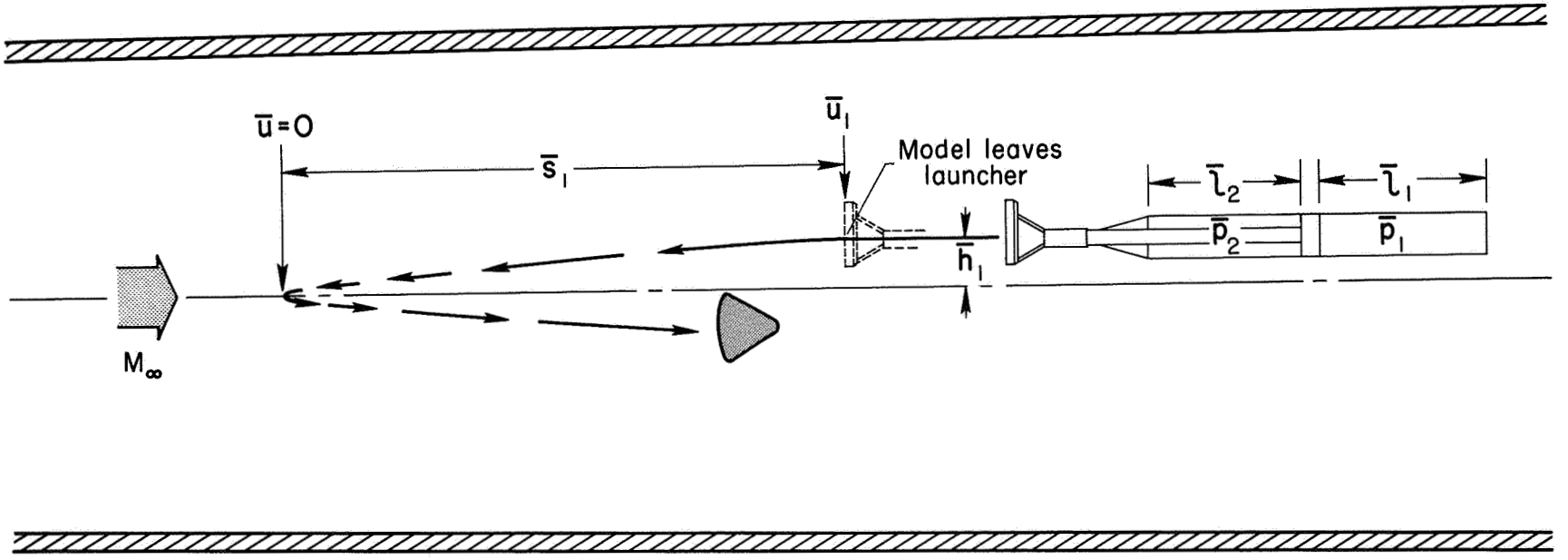

Figure 15.- Schematic drawing of model launcher and free-flight trajectory.

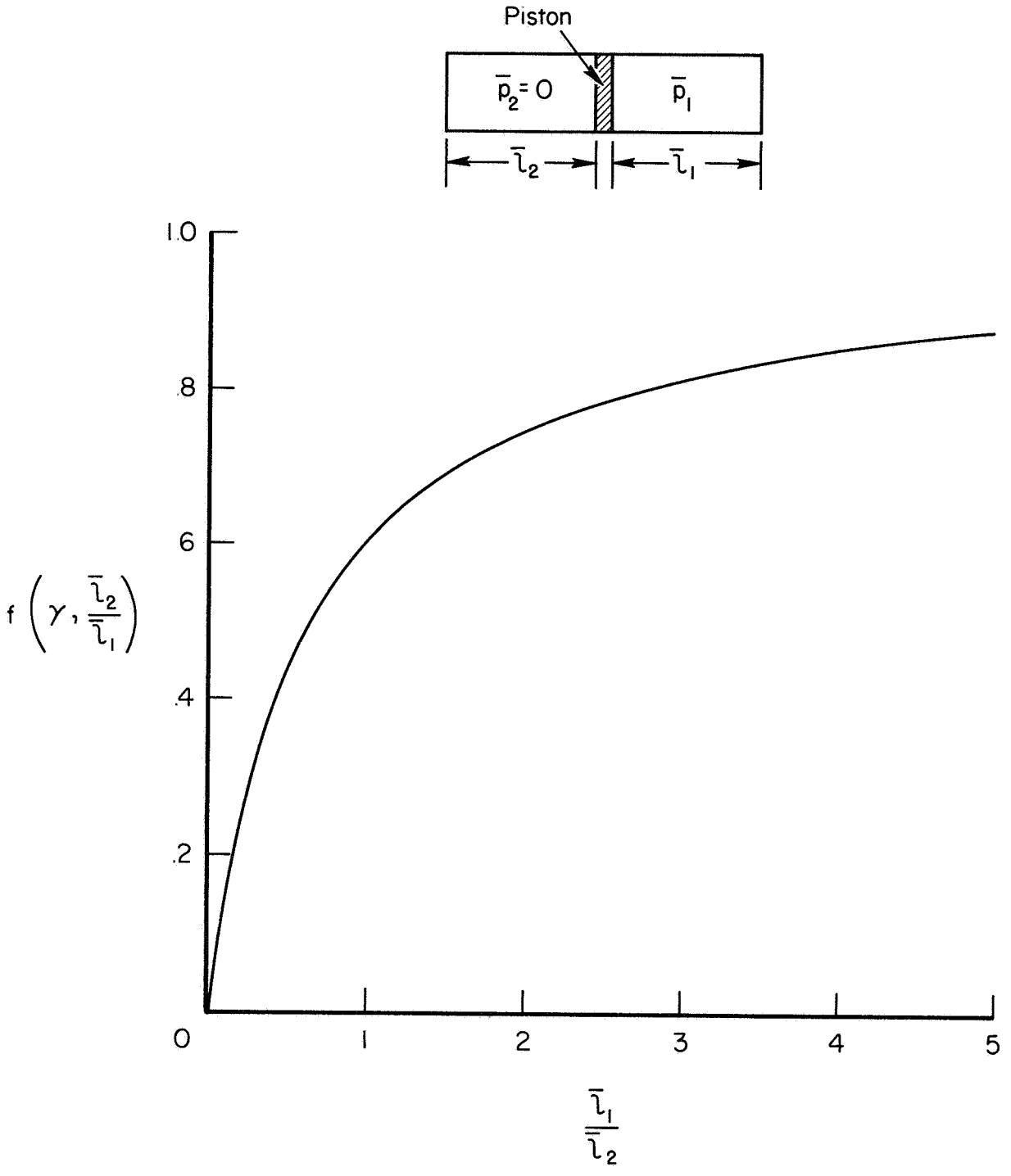

Figure 16.- Variations of the energy function, $f[\gamma,(l_2/l_1)]$, for various ratios of reservoir length to piston stroke, l_2/l_1.

NASA-Langley, 1965 A-2172